Observation of Epitaxially Ordered Twinned Zinc Aluminate "Nanoblades" on *c*-Sapphire

E. McGlynn[a,] *, B. Twamley[b], K.K. Nanda[a,] **, J. Grabowska[a], R. T. Rajendra Kumar[a,] ***, S.B. Newcomb[c], J.-P. Mosnier[a], M.O. Henry[a],

[a]School of Physical Sciences / National Centre for Plasma Science and Technology, Dublin City University, Ireland

[b]School of Chemical Sciences, Dublin City University, Ireland

[c]Glebe Scientific Ltd., Newport, Co. Tipperary, Ireland

*Corresponding author. Tel.: ++353 1 7005387; fax: ++353 1 7005384

Email address: enda.mcglynn@dcu.ie

**Present address: Materials Research Centre, Indian Institute of Science, Bangalore 560 012, India

***Present address: Department of Physics, Bharathiar University, Coimbatore 641 046, India

Keywords:

Zinc aluminate, spinel, epitaxy, sapphire, growth, SEM, nanostructures.

Abstract

We report the observation of a novel nanostructured growth mode of the ceramic spinel zinc aluminate grown on *c*-sapphire in the form of epitaxially ordered twinned crystallites with pronounced vertically aligned “nanoblades” on top of these crystallites. The nanostructures are formed on bare *c*-sapphire substrates using a vapour phase transport method. Electron microscopy images reveal the nanostructure morphology and dimensions and allow direct and indirect observation of the twin boundary location in a number of samples. The nanoblade structure with sharply rising sidewalls gives rise to a distinctive bright contrast in secondary electron images in scanning electron microscopy measurements.

1. Introduction

Growth of functional oxide materials is an important research topic for applications including photonics, catalysis, biocompatibility, high temperature electronics (HTE) and transparent conducting oxides (TCO) [1, 2]. Spinel materials (with chemical formulae AB_2O_4) and their growth mechanisms and structural properties have thus been widely studied. The spinel zinc aluminate ($ZnAl_2O_4$) is of particular technological interest, due to its wide potential functionality [3]. More recent reports have used zinc aluminate to demonstrate a novel technique for core-shell nanostructure synthesis via the nano-Kirkendall effect, and this material shows great promise for nanoscale applications [4]. Zinc aluminate also has a wide bandgap (~3.8 eV) which may lead to applications in

TCO and HTE, and can be doped with rare-earth elements offering the possibility of functioning as a material for phosphors [5, 6]. Zinc aluminate is also a candidate material for optical coating applications and is currently employed in catalysis for applications such as cracking, saturated alcohol dehydration, methanol and other alcohol synthesis and as a catalytic support [7, 8]. The catalytic functionality of sub-micron particles is strongly affected by microstructure, with different facets showing differences in catalytic activity [9]. For this reason ordered growth of micro- or nanostructured catalytic material on robust substrates is an important applied research focus.

We report electron microscopy measurements of a novel nanostructured growth mode of zinc aluminate on *c*-sapphire at lower temperature and/or shorter growth duration in the form of epitaxially ordered twinned crystallites topped with pronounced vertically aligned "nanoblades" which differs substantially from the growth mode at higher temperature for longer growth duration. In the latter case the nanoblades are not observed although twinned crystallites remain. The nanoblade structure's sheer sidewalls lead to a distinctive bright contrast in secondary electron images acquired during scanning electron microscopy (SEM) measurements.

2. Experimental

Zinc aluminate was grown on bare, uncatalysed *c*-sapphire substrates by vapour phase transport (VPT) using carbothermal reduction of ZnO source powders as a Zn source, and nominal growth temperatures of 950^0C and 1125^0C (which we call lower and higher

temperature growths, respectively) and growth durations of 30 minutes and 60 minutes (called shorter and longer durations, respectively). Samples were characterized by SEM (LEO Stereoscan 440), field emission SEM (FE-SEM: lower resolution system Hitachi S-4300 Field Emission; higher resolution system Hitachi S-5500 in-lens cold-field emission XHR SEM) and transmission electron microscopy (TEM: JEOL2000FX operating at 200kV). Samples for SEM and FE-SEM were in most cases sputter-coated with a 10 nm Au layer prior to study to reduce charging effects, though some samples were examined without such a coating. The full details of the growth procedures and sample preparation process for TEM measurements is outlined in our earlier work [10, 11].

3. Results and discussion

In the majority of the following we will confine our attention to samples either grown at ~ 950^0C for 30 minutes duration or those grown at 1125^0C for 60 minutes duration where the key features of both sample types are clearly distinguishable. Another scenario was also used, i.e. growth at 1125^0C for 30 minutes duration, which represents a useful and informative intermediate case and which will be discussed in the latter part of this section in terms of its relevance to the understanding of the overall growth process. Initially we will summarise our results obtained primarily with SEM, the lower resolution FE-SEM system and TEM. More details are available in reference 11.

Figure 1 shows plan-view SEM of samples grown at ~ 950^0C for 30 minutes duration and 1125^0C for 60 minutes duration. For the sample grown at ~ 950^0C for 30 minutes

duration prominent structures with a linear appearance are seen with a high secondary electron contrast, aligned in three specific in-plane directions with respect to the sapphire with an angle of 120° between them. These structures are uniformly distributed among these directions. The long axes of the structures are parallel to equivalent <10-10> sapphire in-plane directions in all cases. For samples grown at ~ 1125^0C for 60 minutes duration the strong contrast of the central line portion of the microstructure is gone, although the three-fold symmetry of micro-structures remains apparent and a clear faceting of the structures is now apparent. The long axes of the structures are again parallel to the <10-10> in-plane directions, in all cases.

Figure 2 shows cross-section and plan-view TEM data for samples grown at ~ 950^0C for 30 minutes duration (a, b) and 1125^0C for 60 minutes duration (c). For the sample grown at ~ 950^0C for 30 minutes duration, a coarse zinc aluminate grain surrounded by a thinner and randomly oriented aluminate region is observed in cross-section in figure 2(a) for the sample grown at ~ 950^0C for 30 minutes and each such coarse grain shows an epitaxial relationship with the sapphire substrate and also shows the presence of at least one twin boundary. The coarse grain does not show a very clear faceting and the top of the grains show no faceting or features which could be definitely correlated with the high contrast SEM features. The twin can be more clearly seen in plan-view in figure 2(b). Electron diffraction shows that the twin plane is an aluminate (111) plane, and the epitaxial relationship is: [10-10] Al_2O_3 // [011] $ZnAl_2O_4$ and (0001) Al_2O_3 // (-2-11) $ZnAl_2O_4$ [11]. This epitaxial and twinning relationship indicates that the intersection of the twin boundary of the aluminate grain with the surface is a line parallel to the sapphire [10-10]

in-plane direction, i.e. exactly parallel to the long direction of the bright symmetric structures seen in SEM. Thus, despite the lack of correlation of detailed grain features such as faceting from initial cross-section TEM with the SEM bright contrast, an identification of the large, twinned, zinc aluminate grains with the bright symmetric structures seen in SEM, and specifically the bright central line region seen in SEM with the twin boundary region is justified. For the sample grown at ~ 1125^0C for 60 minutes duration a largely similar structure is seen in cross-section, i.e. a coarse zinc aluminate grain surrounded by a thinner and randomly oriented aluminate region is observed in cross-section in figure 2(c) and each such coarse grain shows an epitaxial relationship with the sapphire substrate and also shows the presence of at least one twin boundary. The similarity of this structure indicates that the coarse grains in samples grown at ~ 1125^0C for 60 minutes are similar structures to those seen in samples grown at ~ 950^0C for 30 minutes, with differences due to the different processing temperature and duration. In this case however the coarse grain shows a very clear faceting and the top of the grains show clear faceting which clearly correlate with the SEM features in e.g. figure 1(d). Electron diffraction shows that the twin plane is an aluminate (-211) plane in this case (different to the situation for samples grown at 950^0C for 30 minutes), and the epitaxial relationship is: [1-210] Al_2O_3 // [-211] $ZnAl_2O_4$ and (0001) Al_2O_3 // (111) $ZnAl_2O_4$ [11]. Once again these epitaxial and twinning relationships indicate that the intersection of the twin boundary of the aluminate grain with the surface is a line parallel to the sapphire [10-10] in-plane direction, parallel to the long direction of the symmetric structures seen in figures 1(c) and 1(d) supporting the identification of the large, twinned, zinc aluminate

grains with the symmetric structures seen in SEM and the identification of the features seen at the two growth conditions as being similar.

One key point left unresolved by the SEM, lower resolution FE-SEM and TEM images is the origin of the very bright secondary electron contrast seen in samples grown at ~ 950^0C for 30 minutes duration and the lack of observed faceting or features in TEM studies which could be definitely correlated with the high contrast SEM features. The strong secondary electron contrast of the samples grown at lower temperature suggests a very sharp topographic feature at the twin boundary not clearly seen in any of our initial electron microscopy (or possibly other effects such as charging, channelling effects due to the twin boundary or the presence of a sharp nanostructure of different material composition). The topographic origin is hinted at from lower resolution FE-SEM data in the inset of figure 1(e) (the secondary electron signal varies across the bright structure and is brightest at the edges, consistent with a topographic feature with sheer sidewalls) and in figure 1(f) where the tilted view shows evidence of a 3-D nature with sidewalls, but poor resolution makes detailed conclusions impossible. The other possibilities were systematically ruled out based on the persistence of the strong contrast under a variety of analysis conditions and composition analysis via energy dispersive x-ray and x-ray diffraction, further confirmed by the data shown in figures 4(a) and 4(b) below.

Thus we re-examined these structures with a higher resolution FE-SEM system, focussing on the topographic structure in the region of the high secondary electron contrast in samples grown at ~ 950^0C for 30 minutes duration. Higher resolution FE-SEM

of these high electron contrast structures is shown in figure 3, including both plan-view (3(a)) and tilted views (3(b) at ~ 30^0 tilt angle). The plan-view shows a similar pattern of 3-fold symmetric structure and secondary electron contrast to that shown in figure 1 and in the inset the sputtered Au can be discerned in the form of small nanoparticle clusters, while the variation in contrast, with bright edges, is also consistently observed. The tilted view in figure 3(b) establishes unambiguously the 3-D nature of the feature, with sheer sidewalls clearly visible and the structure has the form of a narrow nanoblade protruding vertically from the substrate with evidence of faceting which is most pronounced at the ends of many/most nanoblades which show a re-entrant facet intersecting the substrate plane (see also the inset of figure 1(f)). The latter feature gives the structures an appearance somewhat similar to that of the replaceable blades with an isosceles trapezoidal shape used in some types of utility knives / boxcutters, hence our use of the term “nanoblades” to describe the structures. The Au-coated nanoblades are ~ 30 nm wide, ~ 150 nm high, and with lengths varying in the range of several 100 nm. The very sharp morphology fully explains the bright secondary electron contrast in SEM and its persistence under a range of tilt angles (up to values > 30^0) as due to the combination of the strong topographical tilt and edge effects [12]. The structures seem mechanically quite fragile, and occasional examples of “broken off” structures or sections are seen, one of which is shown in the circled region of figure 3(a). These broken sections allow us to confirm the measurements above from tilted views and the absence of differential bright contrast in the broken off section lying flat (except at the edges due to topography) suggests that the nanoblade is the same aluminate material which makes up the large twinned grains. This will be further discussed below. Occasionally structures of the

nanoblade type are seen in plan-view SEM which show secondary electron contrast which is bright for a portion of the blade length and then disappears, an example of which is shown in figures 3(c) and 3(d) using the higher resolution FE-SEM system. These data show clearly that the upper right hand region has sheer sidewalls characteristic of a nanoblade and giving rise to the bright topographic contrast characteristic of the nanoblade structures in SEM. The lower left hand region is essentially buried in the surrounding deposit and the sheer sidewalls are buried and thus the topographic contrast is lost in this region. These data confirm the assignment of the bright secondary electron contrast in SEM to the nanostructure morphology, specifically to the pronounced topographical tilt and edge effects mentioned above.

The mechanical fragility of the nanoblade structures explains why these were not seen in the cross-sectional TEM data presented earlier, because the TEM sample preparation process would very likely have led to removal and substantial damage to these structures. The coarse grains and lack of clear faceting at the top of the grains mentioned previously is fully consistent with mechanical damage and removal of the nanoblades. In order to examine the details of the structures we applied an adhesive tape to the surface of the sample shown in figure 3(a) and then removed it to deliberately cause mechanical damage. The results are shown in figures 3(e) and 3(f). Examples are seen of torn off nanoblades and nanoblades with the sputtered Au coating removed (which in some cases allows us to measure the nanoblade width at ~ 20 nm without the Au present as in figure 3(e)). In the case of both figures 3(e) and the inset of 3(f) a portion of the underlying, bare nanoblade is clearly visible and a very narrow straight line runs lengthwise down the

very centre of the top of the blade and this line also is seen in the right-hand region of the inset of figure 3(f), where the blade has broken off. We identify this with the twin boundary, identified in the TEM data. This finding provides further support for the claim that the nanoblade is the same aluminate material which makes up the large twinned grains and is an extension of the underlying twinned grains. We also note that the data in figures 3(c) and 3(d) above show indirect evidence for the presence of a twin boundary because the sputtered Au clusters show a symmetrical arrangement along the structure with a "gap" running down the middle, indicative of the effect of the twin on the Au deposition in that region (we note however that this is not always seen for Au-sputtered nanoblade structures, see e.g. the inset of figure 3(a)). We do not have TEM data on nanoblades and thus cannot comment definitively on whether these structures are twinned single crystals or poly-crystalline. However, the TEM data from figure 2 indicate that the underlying twinned grain is single crystalline. If, as above, the blade is an extension of the underlying twinned grains one would expect it to also be a twinned single crystal. The very straight appearance of the twin boundaries in figures 3(e) and 3(f) supports this.

We have also use backscattered electron (BSE) imaging on the broken (and thus with Au coating partially removed) nanoblades shown earlier in figures 3(e) and 3(f), in high angle (HA) mode, shown in figures 4(a) and 4(b), respectively, to look for any evidence of changes in the material composition of the nanoblade structures compared to the surrounding aluminate deposit. No change in composition is apparent in the nanoblades, despite the fact that the fractured nanoblade in figure 4(a) is effectively being viewed at a variety of depths due to the undulating nature of the breakage. Thus there is no evidence

from BSE imaging for any changes in the material composition as a function of depth through the nanoblade nor, furthermore, for any changes in the nanoblade material composition compared to the substrate zinc aluminate (in the lower right hand regions of figures 4(b) the bare substrate is visible). Hence these data strongly indicate that the nanoblade composition is zinc aluminate throughout and an extension of the underlying twinned grain, consistent with the discussions above and below.

Finally, there is a very pronounced topographical difference between samples grown at 950^0C for 30 minutes duration and those grown at 1125^0C for 60 minutes duration, as commented upon above. The samples grown at lower temperature and/or for shorter durations show the presence of nanoblades, whereas those grown at higher temperatures for a longer duration show no evidence of nanoblades and only three-fold symmetric micro-structures with a clear faceting consistent with the large underlying twinned aluminate grains. The conditions which lead to the growth of structure with a morphology as unusual as that of the nanoblades and the evolution of nanoblades into the structures seen at higher temperatures for longer growth duration are of interest. While we have no quantitative model for the nanoblade growth it seems extremely probable that the twin boundary is crucial. We previously showed that the growth of these large aluminate grains and nanoblades is critically dependent on the presence of extended defects in the starting substrate material and that they were seen only in such defective regions [11]. The initial stage of growth deposited Zn/ZnO will grow in a locally different fashion close to positions on the substrate where extended defects intersect the surface, due to local alterations in the surface structure and may grow in a twinned fashion in such

regions, leading to the characteristically twinned zinc aluminate grains after reaction with the sapphire. Following this the twin may then act as a preferential site for Zn nucleation during the first stages of growth (in a manner similar to other defects which intersect a substrate surface, such as dislocations [13, 14]). In this regard we note (a) that bare sapphire surfaces with few or no defects do not provide energetically suitable accommodation sites for nucleation and growth of Zn/ZnO [15] (this is also evidenced by the much smaller film thickness of polycrystalline zinc aluminate when we use sapphire substrates with much lower defect content for growth) and (b) the corresponding absence of evidence for nanoblades or twinned aluminate crystallites in these samples [11]. That the twin can influence deposit nucleation and growth can also be seen in the fact that it clearly affects the Au deposition as shown in figures 3(c) and (d), though in that case it seems to be a less preferred nucleation site. These points all indicate that an enhanced deposition rate may prevail locally in the region of the twin boundary. The twin boundary will also enable enhanced diffusional transport for source material to the sapphire – aluminate interface, leading to much higher reaction and growth rates close to twin boundaries, as seen in our samples – this may well apply both for Zn transport from the surface to the buried aluminate sapphire interface and also for Al transport from the sapphire to the upper interface between the Zn/ZnO and aluminate allowing a high local growth rate for the nanoblade region at the twin as well as for the twin grains. In the presence of the twin boundary the diffusional behaviour is likely to be significantly altered from the normal solid phase reaction of ZnO with sapphire and e.g. the traditional Kirkendall effect associated with faster diffusion of the Zn species compared to the Al species may well be quite different in our samples [4, 16].

The evolution of nanoblades into the structures seen at higher temperatures for a longer duration is also of interest. The data shown in figures 3(c) and 3(d) indicate that the evolution may occur due to the overgrowth of nanoblade structures by the surrounding aluminate polycrystalline layer. However this view is challenged by the clearly faceted nature of the structures grown at higher temperatures for a longer duration, which is not seen in the region of overgrown structure at the lower left hand side of the images in figure 3. Lower resolution FE-SEM data for a pair of samples grown under identical conditions (1125^0C growth for 30 minutes) with one sample receiving an additional 40 minute annealing step in argon gas (no source material in tube) are presented in figure 5. These data demonstrate that the sample receiving the additional annealing step displays the facetted microstructure consistent with the longer duration growths and no evidence of nanoblades, and provide strong evidence that annealing effects associated with longer growth durations are the key aspect of the evolution of the nanoblades into the structures seen after higher temperature growth for a longer duration. This is also consistent with the observed changes in twin boundary crystallography mentioned above which imply significant crystalline modification rather than overgrowth. This microscopic mechanism by which this change in morphology occurs is not fully clear but may be due to material transport via evaporation/sublimation at high temperatures, with different facets evolving differently due to varying surface energetics from facet to facet.

4. Conclusions

We have reported electron microscopy observations of a novel nanostructured growth mode of the ceramic spinel zinc aluminate on *c*-sapphire in the form of epitaxially ordered twinned crystallites topped with pronounced vertically aligned “nanoblades”. Our data have revealed the nanostructure morphology and dimensions and allow direct and indirect observation of the twin boundary location in a number of samples. This growth mode differs substantially from that at higher temperature for longer growth duration where such nanoblades are not observed, although twinned crystallites remain. The sheer sidewalls of the nanoblade structures give rise to a distinctive bright contrast in secondary electron images in scanning electron microscopy measurements. Our data show that the nanoblades are zinc aluminate material and have the same alignment and twin boundary crystallography as the underlying twinned aluminate grains.

We conclude that the unusual nanoblade morphology is due in large part to the presence of the open twin boundary which can affect (a) the local nucleation conditions for Zn/ZnO in the earliest stages of growth and (b) the subsequent solid state reactions with sapphire to form zinc aluminate by altering the normal diffusion conditions locally due to the ease of transport of reacting materials along the low density twin boundary. Furthermore we suggest that annealing effects associated with longer growth durations rather than overgrowth of nanoblades by the surrounding aluminate polycrystalline layer are the main driver of the evolution of the nanoblades into the faceted microstructures seen after growth at higher temperatures for a longer duration.

The ability to grow nanostructured ceramic aluminate deposits on specific regions of a substrate surface (e.g. mechanically damaged regions) may give rise to applications in HTE and phosphors (where the nanostructured morphology may affect electronic and optical properties) as well as catalysis (where different facets may show different catalytic activity).

Acknowledgements

We acknowledge financial support from SFI (PI grant # 02/IN1/I95 and equipment funding under Grant No. 03/IN3/1361/EC07), the Irish HEA under the NDP and internal funding from the NCPST, DCU.

Figure Captions

Figure 1: SEM images of samples grown on c-sapphire; (a) growth temperature 950^0C (growth duration 30 minutes); (b) higher magnification of sample in (a); (c) growth temperature 1125^0C (growth duration 60 minutes); (d) higher magnification of sample in (c); (e) lower resolution FE-SEM image of the sample in 1(a) – inset shows the intensity line profile along the dashed line; (f) lower resolution FE-SEM image of the sample in 1(a) tilted at 45^o – inset shows a close-up of a single bright structure.

Figure 2: (a) bright field cross-sectional TEM image from sample grown at 950^0C for 30 minutes; (b) bright field plan-view TEM image from sample grown at 950^0C for 30 minutes; (c) bright field cross-sectional TEM image from sample grown at 1125^0C for 60 minutes. The various labels indicate twin and grain boundaries.

Figure 3: (a) higher resolution FE-SEM plan-view (broken off structure indicated by circled region), inset shows higher magnification image of sample shown in (a); (b) higher resolution FE-SEM tilted view of sample shown in (a) at ~ 30^0 tilt angle; (c) plan-view higher resolution FE-SEM showing structure with varying contrast along its length (inset shows lower magnification image); (d) tilted view (at ~ 30^0) of same structure (inset shows higher magnification image of upper right hand region of nanoblade); (e) and (f) show higher resolution FE-SEM plan-views of sample shown in (a) above, following application of an adhesive tape to deliberately cause mechanical damage.

Figure 4: (a) plan-view higher resolution FE-SEM image of structure in figure 3(e) in HA-BSE mode; (b) tilted view (at ~ 30^0) higher resolution FE-SEM image of structure in figure 3(f) in HA-BSE mode.

Figure 5: lower resolution FE-SEM image of structures grown at 1125 °C for 30 min, showing three-fold symmetric microstructures with high SEM contrast (inset shows a sample grown under identical conditions as that in main figure but with additional 40 min anneal at 1125 °C).

References

[1] D.C.Look, Mater.Sci.Eng. B 80 (2001) 383.

[2] S.J.Pearton, D.P.Norton, K.Ip, Y.W.Heo, T.Steiner, J.Vac.Sci.Technol. B 22 (2004) 932.

[3] S.K. Sampath, D.G. Kanhere, R. Pandey, J. Phys. Condens. Matter. 11 (1999) 3635.

[4] H. J. Fan, M. Knez, R. Scholz, K. Nielsch, E. Pippel, D. Hesse, M. Zacharias, U. Gosele, Nat. Mat. 5 (2006) 627.

[5] R. Pandey, J.D. Gale, S.K. Sampath, J.M. Recio, J. Am. Ceram. Soc. 82 (1999) 3337.

[6] B. Cheng, S. Qu, H. Zhou, Z. Wang, Nanotechnology 17 (2006) 2982.

[7] T. El-Nabarawy, A.A. Attia, N. Alaya, Mater. Lett. 24 (1995) 319.

[8] J. Wrzyszcz, M. Zawadzki, J. Trawczynski, H. Grabowska, W. Mista, Appl. Catal. A 210 (2001) 263.

[9] P.L. Hansen, J.B. Wagner, S. Helvig, J.R. Rostrup-Nielsen, B.S. Clausen, H. Topsoe, Science 295 (2002) 2053.

[10] J.Grabowska, K.K. Nanda, R.T. Rajendra-Kumar, J. P. Mosnier, M.O. Henry, S. B. Newcomb, P. McNally, L. O'Reilly, X. Lu, E. McGlynn, Superlatt. Micro. 42 (2007) 327.

[11] J. Grabowska, R.T. Rajendra Kumar, E. McGlynn, K.K. Nanda, S.B. Newcomb, P.J. McNally, L. O'Reilly, J.-P. Mosnier, M.O. Henry, Thin Solid Films 516 (2008) 1725.

[12] L. Reimer, Scanning electron microscopy: physics of image formation and microanalysis, 2nd edition, Springer (Berlin), 1998.

[13] J. G. Lozano, A. M. Sánchez, R. García, D. González, D. Araújo, S. Ruffenach, O. Briot, Appl. Phys. Lett. 87 (2005) 263104.

[14] W.K. Burton, N. Cabrera, F.C. Frank, Phil. Trans. Royal Soc. A, 243 (1951) 299.

[15] R.B. Saunders, E. McGlynn, M. Biswas, M.O. Henry, Thin Solid Films 518 (2010) 4578.

[16] D.B. Holt, B.G. Yacobi, Extended Defects in Semiconductors, Cambridge University Press (Cambridge), 2007, page 353.

Figure 1:

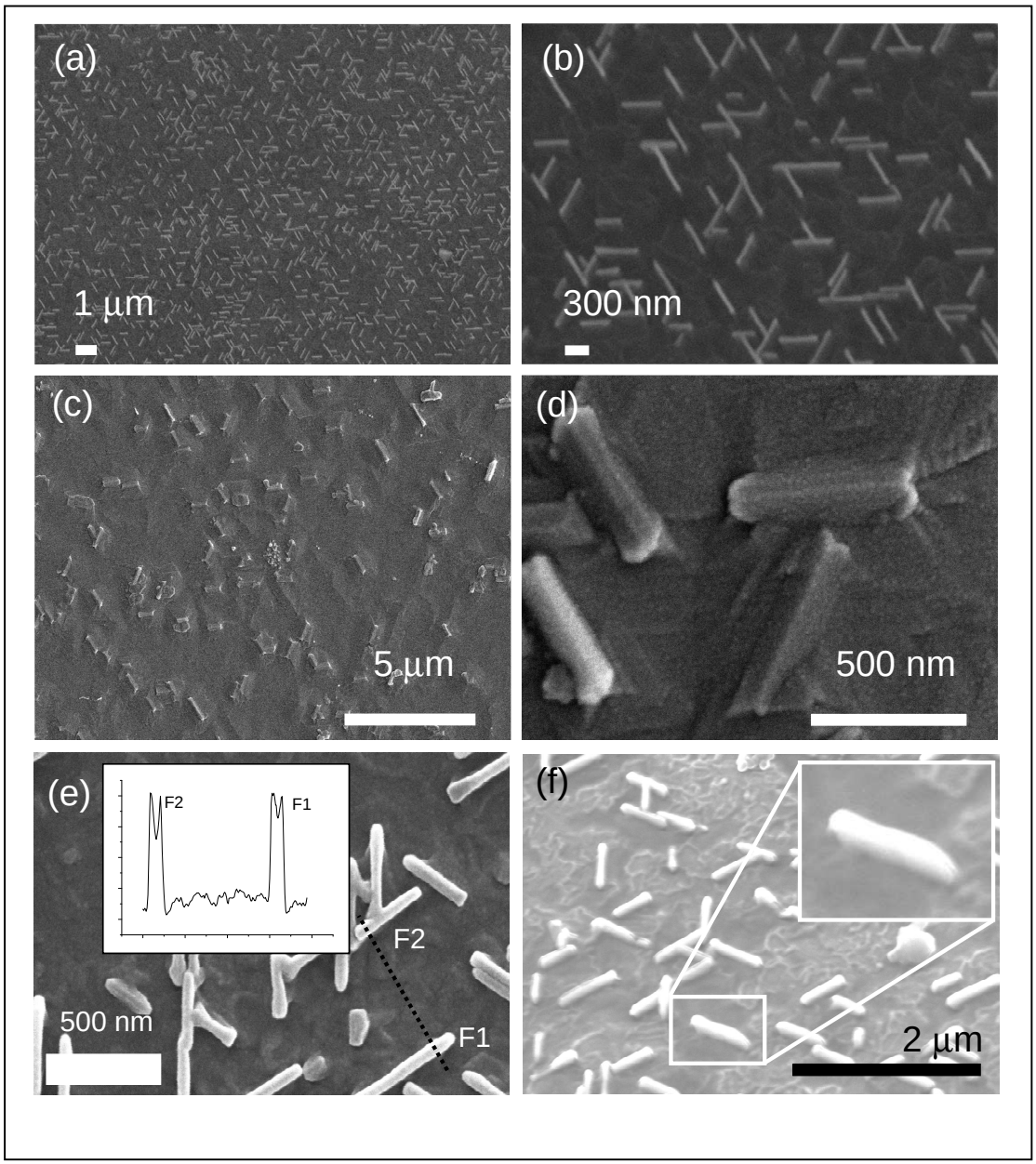

Figure 2:

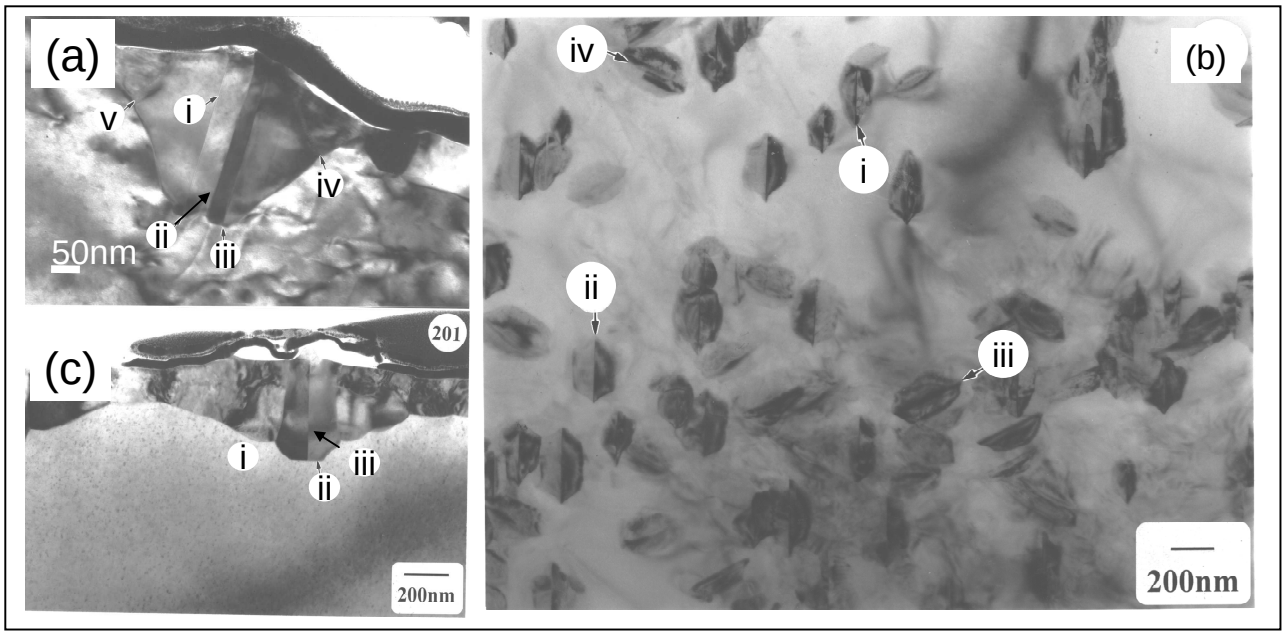

Figure 3:

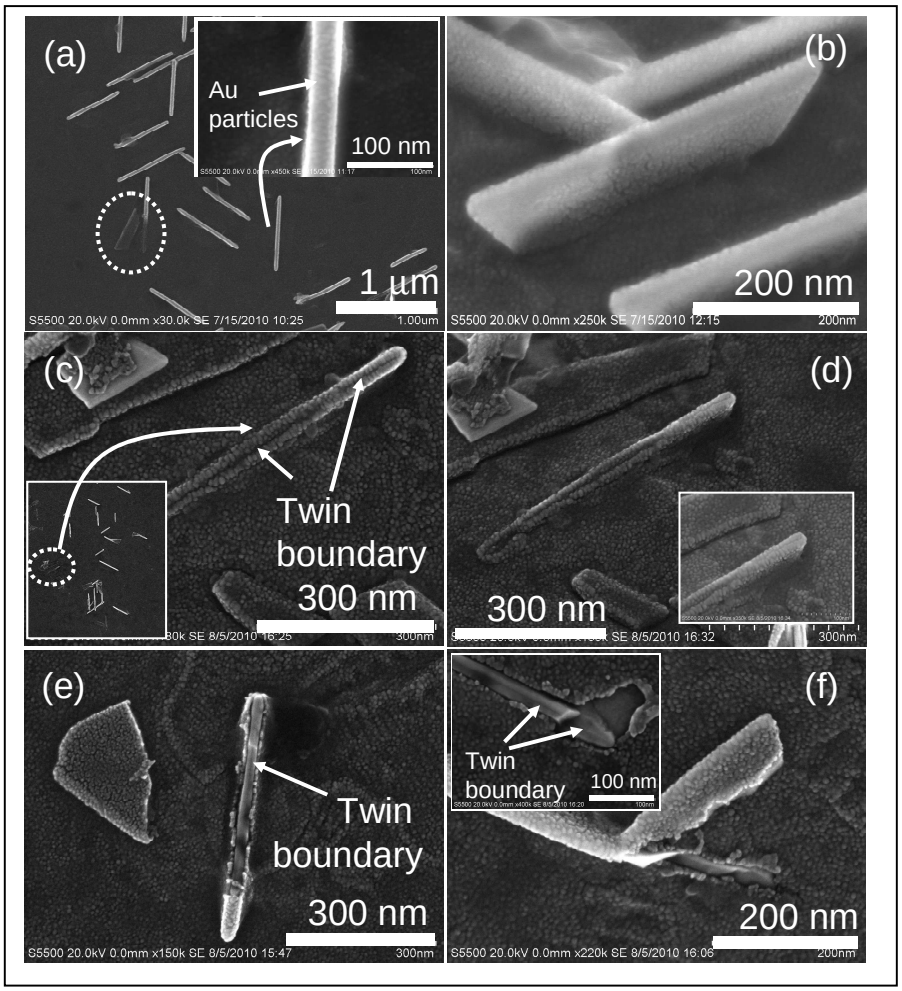
(a)
Au
particles
100 nm
1 µm
S5500 20.0kV 0.0mm x30.0k SE 7/15/2010 10:25
1.00um
(b)
200 nm
S5500 20.0kV 0.0mm x250k SE 7/15/2010 12:15
200nm
(c)
Twin
boundary
300 nm
(d)
300 nm
SE 8/5/2010 16:32
300nm
(e)
Twin
boundary
300 nm
S5500 20.0kV 0.0mm x150k SE 8/5/2010 15:47
300nm
(f)
Twin
boundary
100 nm
200 nm
S5500 20.0kV 0.0mm x220k SE 8/5/2010 16:06
200nm

Figure 4:

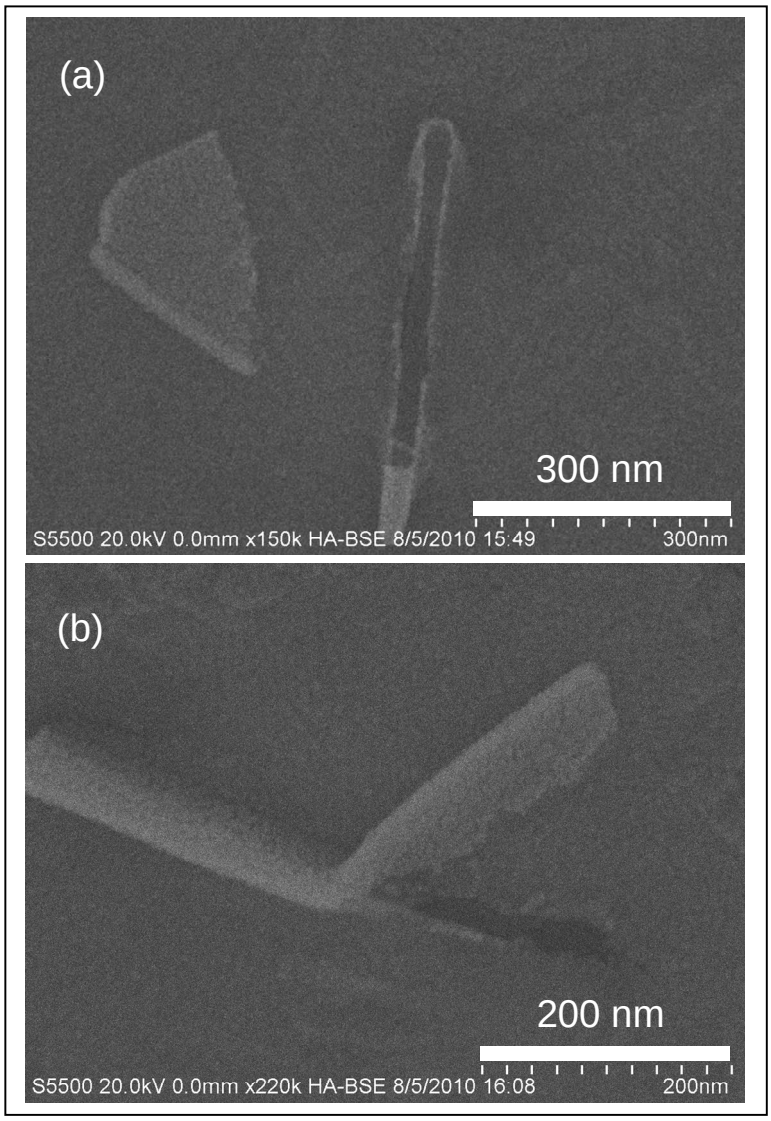
(a)
300 nm
S5500 20.0kV 0.0mm x150k HA-BSE 8/5/2010 15:49
300nm
(b)
200 nm
S5500 20.0kV 0.0mm x220k HA-BSE 8/5/2010 16:08
200nm

Figure 5: